A CMOS Image Sensor with In-Pixel Temperature Sensors for Dark Signal Non-Uniformity Compensation

Shuang Xie[1]
[1]Electronic Instrumentation Laboratory
Delft University of Technology
Delft, the Netherlands

Accel Abarca Prouza[1]
[1]Electronic Instrumentation Laboratory
Delft University of Technology
Delft, the Netherlands

Albert Theuwissen[1,2]
[2]Harvest Imaging
Bree, Belgium

***Abstract*—This paper presents a CMOS image sensor with in-pixel temperature sensors, for dark signal non-uniformity (DSNU) compensation between -20 ºC and 80 ºC. Two types of in-pixel temperature sensors, either based on a BJT or on the in-pixel source follower (SF) itself, are implemented, measured and compared, both implemented inside a 64×64 CIS array fabricated using 0.18 µm technology. Both temperature sensors achieve inaccuracies less than ±0.3 ºC, between -20 ºC and 80 ºC, when measured on 3 test chips. Dark current measured on the neighboring image pixels of the two types of temperature sensors show that the SF based one incurs no penalty to the image sensor array, while the BJT based alternative can introduce 100 times more dark current to its surrounding pixels. Using the temperature information provided by the in-pixel temperature sensors, the average dark current can be predicted and compensated by at least 70 %, on 3 measured chips.**

I. INTRODUCTION

This paper introduces a proof-of-concept CMOS image sensor (CIS) equipped with the capability to measure the temperature in each pixel and to digitally compensate for dark current increment with the temperature. The compensation method, in general, is to capture a dark frame at room temperature (e.g., at the factory) and with the temperature information, the dark current and DSNU at a different temperature can be locally predicted and compensated. Previous efforts to incorporate temperature sensors inside a CIS have been published in [1][2]. Meantime, a digital FPN compensation method has been proposed in [3]. Compared to the aforementioned publications, this paper proposes reusing the 4T PPD CIS image pixels as temperature sensors, without incurring any penalty to the CIS's area, power or any other performance, as the CIS array keeps its homogeneousness.

In contrast, the incorporated BJT temperature sensors in [1][2] incur 3 times more dark current, compared to when without the incorporated BJT temperature sensors, despite that in [1][2] the BJTs are disconnected from the column bus during the image capture. In addition, forward biased BJT temperature sensors are reported to incur electron luminescence (EL) as a light emitting diode (LED) in [4]. Besides, dark current is observed to bloom (to neighbouring pixels) in [5]. To further investigate the trade-offs between thermal sensing accuracy and performance penalties for the BJT and the imager based temperature sensors, 6 BJT based temperature sensors (with a spatial density of 128:1) are implemented inside a CIS array, which are compared to a pixel-SF-based alternative that can be reconfigured for temperature measurement in each pixel (MOS based). Each sensor occupies an area of 11 µm ×11 µm, the same as an image pixel. Dark current is measured on the incorporated BJTs' neighbouring image pixels and compared with the case without the incorporated heterogeneous device. Both temperature sensors achieve accuracy better than ±0.3 ºC for 3 test chips, although the SF based has slightly better 3 σ accuracy of ±0.65 ºC, compared to ±0.75 ºC for the BJT based alternative. Furthermore, the latter (BJT) could incur 100 times more dark current to its neighbouring pixels and 50 % more dark signal non-uniformity (DSNU) to the whole array (exclusive of the BJTs and their 8 ambient rows of hot pixels). Compared to [1][2], in this work, the average dark current are compensated by at least 70 %, using the temperature information. This paper is organized as follows. Section II describes the operating principles of the BJT and the MOS based in-pixel temperature sensors. Section III shows the measurement results of the temperature sensors as well as the average dark current versus temperature, with and without and imbedded in-pixel BJTs, along with the thermal prediction and compensation of dark current based on temperature sensors' outputs. Section IV concludes this paper.

II. Operating Principle

A. BJT based temperature pixel

Fig. 1 shows the schematic of the in-pixel BJT based temperature sensor. Compared to the previously published work in [1][2], the pMOS based source follower has been removed for three purposes. First of all, Q1, or the entire cell's output impedance is approximately $1/g_{mQ}$, where g_{mQ} (e.g., a few dozens of µA/V), is the transconductance of Q1 and is normally not less, if not larger than that of a MOS based SF. Secondly, the total temperature pixel area has been reduced to that of one pixel pitch in this design, compared to two in [1][2]. The last but not the least, a pMOS SF implemented in an n-well provides additional parasitic photodiode and considerably lowers the quantum efficiency of the pixels. Measurement results will be provided in Section III to support this statement. The timing diagram of the proposed temperature sensors is shown in Fig. 2: During $T_{CDS,1}$ and $T_{CDS,2,}$ the BJT biasing current is $I_{1,1}$ and $I_{1,2}$, accordingly, and the temperature pixel output is $V_{BE,1}$ and $V_{BE,2}$, whose difference ΔV_{BE} is amplified by the programmable gain amplifier (PGA) [1]. The in-pixel temperature sensors share the column and the row buses with the image pixels. As indicated in Fig. 1, the differential pixel output ΔV_{BE} at column (j) biased at sequential ratiometric currents I_{bias} (Fig. 1), between two phases, is:

$$\Delta V_{BE} = V_{BE,1} - V_{BE,2} = \frac{kT}{q}\ln(N) \qquad (1)$$

while T is the absolute temperature, and q is the electrical charge magnitude. N is the current ratio that is set precisely by the dynamic element matching (DEM) circuit.

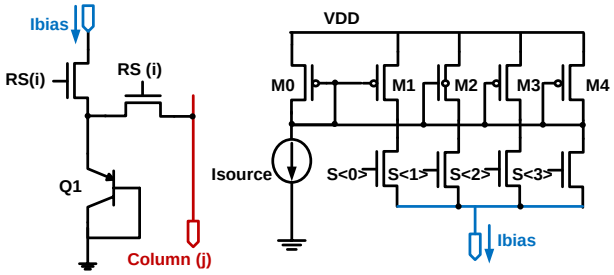

Fig. 1 Schematic of in-pixel BJT based temperature sensor and its current biasing with DEM.

B. 4T PPD imager based temperature sensor

The source-follower-based temperature sensor's schematic is shown in Fig. 3. Its timing diagram and column readout circuits are identical to that of the image pixels, except that the reset *RST* has to be on and its gate voltage level has to meet the condition of: $V_{RST} > V_{PIX} + V_{TH}$ (V_{TH} is the threshold voltage of M_{RST}) for thermal sensing. Then, the M_{SF} gate voltage V_{FD} equals that of V_{PIX_SUP} and the pixel output voltage $V_{PIX} = V_{PIX\_SUP} - V_{GS}$ (V_{GS} is the gate-source voltage of M_{SF}) if ignoring the voltage drop on M_{RS}. One has to ensure that TG is off to avoid disturbance into the V_{FD} node in case of light input. When biased in subthreshold region, an nMOS transistor has an I-V characteristic similar to that of a BJT device, except for a subthreshold voltage element. Therefore, the differential pixel output voltage ΔV_{BE}, at V_{PIX}, when biased with sequential ratiometric currents $I_{1,1}$ and $I_{1,2}$ (Fig. 2), between two phases, is:

$$\Delta V_{GS} = V_{GS,1} - V_{GS,2} = n\frac{kT}{q}\ln(N) \qquad (2)$$

One may notice the similarity between equation (1) and (2) except for an "*n*" factor, which is process dependent. One significant difference in the designer's perspective is that the BJT based sensor requires a current source while the SF based one requires a current sink, which is the same as that in the image pixels. In other words, the current biasing for the BJT based type requires additional design and layout complexity while the latter does not.

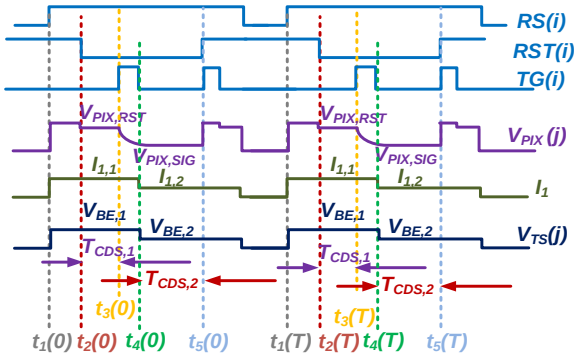

Fig. 2 Proposed temperature sensors' timing diagram

III. Measurement Results

A. In-pixel temperature sensors

A 64×64 CIS prototype is fabricated using 0.18 µm technology inside a CIS array, with 6 imbedded BJT based temperature sensors. Its micrograph is shown in Fig. 4, indicating a pixel pitch of 11 µm. The 64 column PGA/CDS analog outputs are digitized by a 16-bit on-board analog-to-digital converter (ADC) (AD9826) and read out by CameraLink and Labview into an Excel file, which is further processed in MATLAB. The resolution of the following measurement results is limited by the ADC, to be 30 µV (or 0.25 °C), with a reference voltage of 2 V. The PGA gain used for measuring temperature sensors are set to be 16, or 24 dB for

the BJT based temperature sensors and its resolution is around 0.04 ºC. Fig. 5 shows both temperature sensors' measured outputs and errors, including curvatures and 3 σ inaccuracies among 3 chips, upon a 2nd order master curve fitting for each type and the a two-point calibration for each sensor at -15 ºC and 40 ºC, respectively.

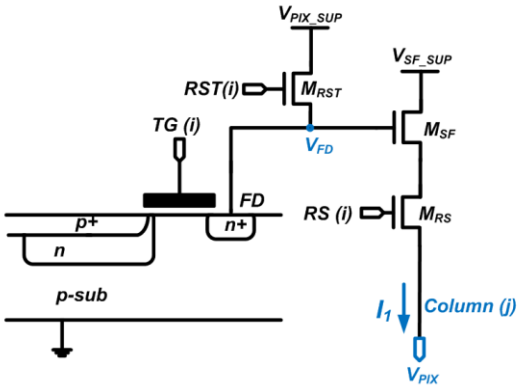

Fig. 3 Schematic of 4T PPD image pixel (SF) based temperature sensor.

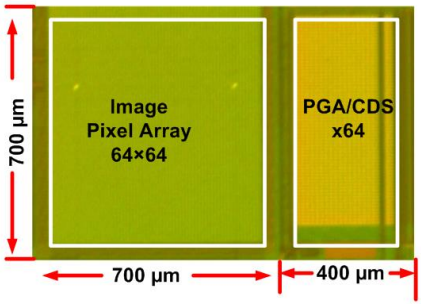

Fig. 4 Micrograph of the proposed CIS with the capabiliy to measure temperature in each pixel. Each block is labelled its function and area. The two invisble lighter spots within the CIS array are 2 of the 10 BJTs implemented.

B. Dark current measurements

To further investigate the effects of in-pixel BJT based temperature sensors on image pixels, the dark current is measured for the whole array, as shown in Fig. 6. The measured dark current is in fact a combination of dark current and EL. It can be seen that the rows next to the BJT based temperature sensors demonstrate almost 100 times larger dark current/EL, compared to that of the average. The increment can be attributed to elevated dark current as well as EL. This deduction is further supported by the fact that, at temperatures below 0 ºC, the measured combined dark current and electro-luminescence is not much higher for rows surrounding the BJTs, as dark current has a much stronger dependence on temperature than the electro-luminescence does. In Fig. 6, it seems that the array without the BJTs has similar dark current level as that with the BJTs. A spatial dark current map measured at 500 ms and 60 ºC is shown in Fig. 7, illustrating visible larger dark current for pixels surrounding the BJTs. Fig. 8 shows the part with the BJTs not only demonstrates 10 % larger average dark current and but also has 50 % larger dark signal non-uniformity (DSNU) for the 36 rows in the middle, which are at more than 8 rows' distances from the incorporated BJT. Dark currents are measured on 3 chips and a master (global) exponential fit ($y=a\cdot\exp(bT)$, where T is the temperature, a and b are constants) is applied to predict the dark current. The deviations between the prediction and the measurements results from 3 chips are within ±17 %, as shown in Fig. 9. Taking into considerations the errors of the temperature sensors measured, the average dark current can be corrected by 70 %.

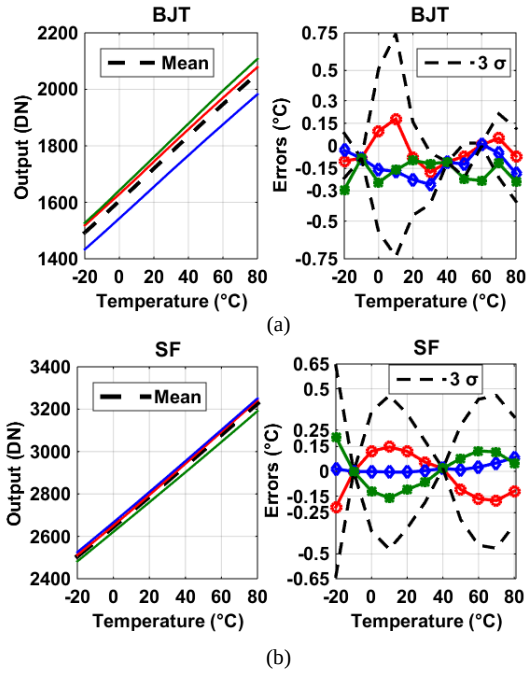

Fig. 5 Measured outputs of the BJT (a) and the SF (b) based temperature sensors, averaged each chip. The measurement errors (curvature) and 3 σ process variations among 3 chips are upon a two-point calibration of each chip at -15 ºC and 40 ºC, and with a 2nd order master curve fitting for each type.

IV. CONCLUSIONS

A CIS targeted for temperature compensation of dark current has been presented in this paper. It is equipped with the functionality to sense temperature in each pixel, using the original 4T PPD CIS imager's SF. The proposed in-pixel temperature sensors can assist digital compensation of dark current by at least 70 % with their measured accuracy. Experimental results show that the SF based type is a better candidate for thermal compensation of dark current, as it incurs no performance penalty (e.g., DSNU, dark current) to the CIS, compared to its BJT based counterpart. Table I summaries the performances of both temperature sensors, whose advantages are smaller area and no extra in-pixel hardware (SF based),

compared to previous publications [6], while maintaining reasonable accuracy and figure of merit (FOM) [7].

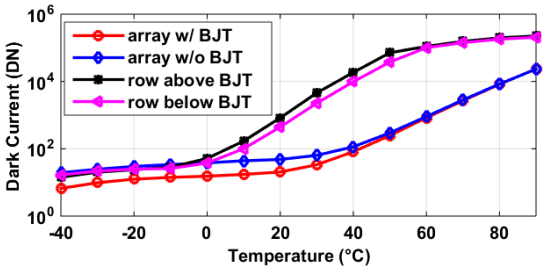

Fig. 6 Measured dark current of the same chip that implements the BJT based temperature sensors of sections II.A.

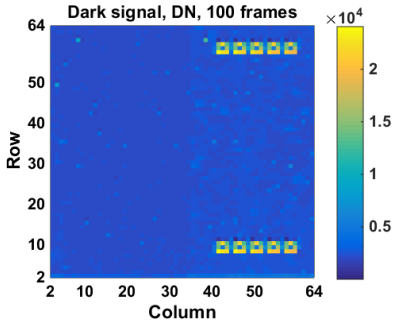

Fig. 7 Spatial dark signal in the presence of in-pixel BJT based temperature sensors, at 500 ms and 60 ºC. The surrounding image pixels of the 10 BJTs (8 sensors, 2 test features) show much larger dark current, when averaging 100 images.

TABLE I

Temperature Sensor	This work BJT based	This work SF based	[6]
Process	180 nm CIS	180 nm CIS	180 nm
Temp. Sensor area [µm²]	121	No additional area	89000
Temperature Range (ºC)	-20 to 80	-20 to 80	-20 to 80
Resolution (ºC)	0.04	0.04	0.09
Conversion Time (ms)	400	400	800
Power (µW)	8.3[a]	1[a]	0.8
Resolution FOM (nJ·K²)[b]	5.3	0.64	5.3
3 σ Accuracy	±0.75 ºC	±0.65 ºC	±1 ºC
Rel.IA (%)[c]	1.5	1.3	2

[a]w/o ADC, [b] energy/Conversion×(Resolution)^{2,}, in reference to [7]

[c]3 σ accuracy /temperature range, in reference to [7]

REFERENCES

[1] S. Xie, A. Abarca, J. Markenhof, X. Ge, and A. Theuwissen, "Analysis and calibration of process variations for an array of temperature sensors," *in 2017 IEEE SENSORS*, 2017, pp. 1-3.

[2] A. Abarca, S. Xie, J. Markenhof, and A. Theuwissen, "Integration of 555 temperature sensors into a 64 × 192 CMOS image sensor," Sensors and Actuators A: Physical, vol. 282, pp. 243-250, 2018/10/15/, 2018.

[3] J. M. Margarit, G. Vergara, V. Villamayor, et.al, "A 2 kfps Sub-µW/Pix Uncooled-PbSe Digital Imager With 10 Bit DR Adjustment and FPN Correction for High-Speed and Low-Cost MWIR Applications," *IEEE Journal of Solid-State Circuits*, vol. 50, no. 10, pp. 2394-2405, 2015.

[4] K. Seo, S. Lee, P. Ahn, D. Kim, and K. Cho, "A Study on Photon Effect to Image Plane," *in 2017 International Image Sensor Workshop*, 2017, pp.31.

[5] Jean-Marc Belloir, et.al "Dark Current Blooming in Pinned Photodiode CMOS Image Sensors", IEEE Journal of Solid-State Circuits, vol. 50, no. 10, pp. 2394-2405, 2015.

[6] W. Song, J. Lee, N. Cho, and J. Burm, "An Ultralow Power Time-Domain Temperature Sensor With Time-Domain Delta–Sigma TDC," *IEEE Transactions on Circuits and Systems II: Express Briefs*, vol. 64, no. 10, pp. 1117-1121, 2017.

[7] K. Makinwa, Smart Temperature Sensor Survey, available online at:https://ei.tudelft.nl/smart_temperature/

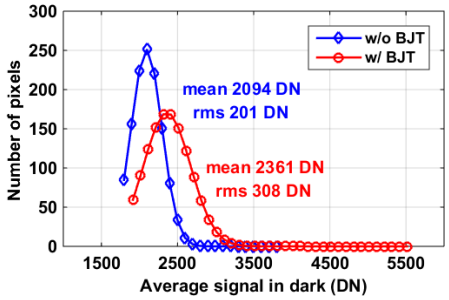

Fig. 8 Dark current and DSNU of Fig. 7, measured on the same chip, containing only the 36 rows in the middle (exclusive of the BJTs and their surrounding 8 rows of hot pixels). The part with BJTs (the right half side) has 10 % larger average dark current and 50 % larger DSNU.

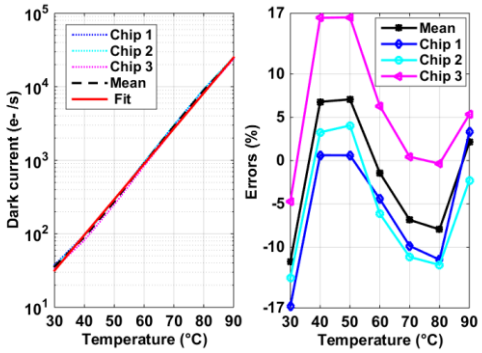

Fig. 9 Measured average dark current for 3 chips and their exponential fit (left) and deviations from the exponential fit (right).

ACKNOWLEGEMENT

The authors acknowledge the support of TowerJazz in realizing the prototype CIS devices. The research is part of the CISTERN and the EXIST projects, funded by the Dutch government through the PENTA and H2020 initiative. The authors would like to thank Prof. Makinwa for advices, Xiaoliang Ge for the image pixel design, Zuyao Chang and Lukasz Pakula for the measurement setups.